SLAC-PUB-2535
AATF/80/23
June 1980
(A/I)

DISRUPTION LIMITS FOR LINEAR COLLIDERS*

Robert Hollebeek
Stanford Linear Accelerator Center
Stanford University, Stanford, California 94305

ABSTRACT

Beam behavior in a single-pass collision device has been investigated using a cloud-in-cells plasma simulation code. The intense electromagnetic fields of the beams produce mutual focusing effects whose strength is determined by the disruption parameter D. The consequent decrease in the beam radii causes an increase in the luminosity of a single collision. The dependences of the beam behavior on beam profiles and current density are described. The beam behavior is stable for several plasma oscillations and indicates that high luminosity can be achieved in single-pass collision devices by using intense beams.

Submitted to Nuclear Instruments and Methods

---

* Work supported by the Department of Energy, contract DE-AC03-76SF00515.

I. Introduction

The idea of using two linear accelerators firing beams of particles at each other for the study of high energy interactions has been suggested by several authors.[1)] This type of device is called a linear collider and is of particular importance in the area of high energy electron-positron physics where the energy loss in a circular machine has become a dominant consideration in the design of new storage rings. For circular machines, modest increases in beam energy are accompanied by large increases in either the power required to run the machine, the size of the machine, or both. Linear colliders can reduce these problems if the beams can be made sufficiently dense at the collision point.

The small emittance of linear accelerator beams allows the beam to be focused to a very small spot (several square microns). For a linear collider, one would like to decrease the spot size as much as possible to increase the luminosity or rate at which interesting interactions occur. However, when two such beams collide, the intense electromagnetic fields of the two beams will cause the beams to be disrupted. If this disruption destroys the beam focus, the luminosity will be decreased.

If the beams consist of short pulses, and each pulse is discarded after a collision (single-pass collision device), then the growth of instabilities due to this beam-beam interaction will be limited by the short duration of the interaction. The limitations on beam intensity in a single-pass collision device will be determined by the plasma effects which occur during the short collision time.

This paper presents the results of investigations into the behavior of the two beams in a single-pass collision device. There are two issues

which must be addressed in considering the beam-beam interaction in such a device. The first is, how large can the transverse density of the beams be before plasma instabilities increase the size of the beams during the collision and thereby reduce the luminosity? The second question is, what is the effect of the beam-beam dynamics without instabilities on the average luminosity of a collision?

The beam-beam dynamics have been investigated using a modified three-dimensional cloud-in-cells (CIC) plasma simulation program. These studies indicate that the number of plasma oscillations during beam passage is of order

$$n \approx \frac{1}{3}\sqrt{D} \tag{1}$$

where D is the dimensionless disruption factor (discussed later) which is related to the initial beam density. Typical instability growth rates are such that n values of one or two can be achieved allowing quite large values of D.

The second result of these studies is that the pinch effect due to the attraction of the oppositely charged beams enhances the luminosity. Figure 1 shows the changes which occur in two such beams as they collide. The luminosity is related to an overlap integral of the density distribution of the two beams. The behavior of the luminosity as a function of initial beam density and beam profile can be studied with plasma simulation techniques and can be reliably calculated for small numbers of plasma oscillations.

The definition of the disruption factor is discussed in Section II and its relation to the plasma frequency and bunch instabilities in Section III. Section IV discusses the computer simulation of the beam-

beam interaction. Section V gives the results of the simulations for the enhancement of the luminosity due to beam pinch. Section VI discusses the case where the beams are offset or have uniform transverse profiles. The conclusions are summarized in Section VII.

II. Beam-Beam Disruption Factor

To investigate the interaction of the two beams as they collide, one must start by looking at the electrodynamics of two relativistic particles traveling in opposite directions. In the rest frame of particle 1, particle 2 approaches with

$$\gamma' \simeq 2\gamma^2 \quad . \tag{2}$$

The fields at the position of particle 1 can be calculated by transforming the Coulomb field of particle 2 in its rest frame to the frame moving with

$$\beta' = \left(1 - \frac{1}{\gamma'^2}\right)^{1/2} \quad . \tag{3}$$

If particle 2 travels along the z axis and has a minimum displacement from particle 1 of b in the x direction (see fig. 2), the electric and magnetic fields are[2)]

$$E_x = \frac{\gamma' qb}{(b^2 + \gamma'^2 v^2 t^2)^{3/2}}$$

$$E_z = \frac{-q\gamma' vt}{(b^2 + \gamma'^2 v^2 t^2)^{3/2}} \tag{4}$$

$$B_y = \beta' E_x$$

The time dependence of the fields is shown in fig. 3. Note that, as γ increases, E_x increases and Δt decreases in such a way that the total impulse given to particle 1 is proportional to 1/v. For electrons with E = 50 GeV, $\gamma = 10^5$ so that at high energies an impulse approximation for the effect of the transverse fields is justified. The impulse is just

$$F\Delta t \sim \frac{e^2}{bc} \tag{5}$$

The total impulse in the longitudinal direction (due to E_z) is zero.

Consider now a test particle with displacement b from the collision axis incident on a charge distribution as shown in fig. 4. For simplicity, let the distribution be a uniform density cylinder with

N = number of particles of charge e

R = radius of the bunch

L = length of the bunch

Then the incident particle sees a magnetic field H_ϕ due to the current caused by the passage of the other beam. The current enclosed by a circular contour of radius b is

$$I = \frac{Ne}{L} \cdot c \cdot \frac{\pi b^2}{\pi R^2} \tag{6}$$

and amperes law gives

$$\oint \underset{\sim}{H} \cdot d\underset{\sim}{l} = \frac{4\pi}{c} I = 2\pi b\, H_\phi \quad , \qquad H_\phi = \frac{2Ne\, b}{LR^2} \tag{7}$$

For oppositely charged beams the force is radial and directed inwards

$$F_r = - \frac{2Ne^2 b}{LR^2} \tag{8}$$

and is experienced for a time $\Delta t = \frac{L}{2c}$.

The effect of the electric field of the passing relativistic bunch is equal to that of the magnetic field ($E_x = \frac{1}{\beta} B_y$) hence the total deflection is given by

$$\Delta r' = \frac{\Delta p_\perp}{p} = \frac{2F_r\, \Delta t}{\gamma mc} = - \frac{2N r_e\, b}{\gamma R^2} \tag{9}$$

A similar analysis applied to a bi-Gaussian distribution gives[3)]

$$\Delta x' = -\frac{2N r_e x}{\gamma\sigma_x(\sigma_x + \sigma_y)}$$
$$\Delta y' = -\frac{2N r_e y}{\gamma\sigma_y(\sigma_x + \sigma_y)} \qquad (10)$$

for displacements $x << \sigma_x$ and $y << \sigma_y$.

The focal length of a thin lens is given by

$$\Delta x' = -\frac{1}{f} x \qquad (11)$$

and comparing this to eqs. (9), (10), one can define a dimensionless parameter, called the disruption factor, which is the ratio of the length of the bunch to the focal length near the center. For a Gaussian distribution,

$$D = \frac{\sigma_z}{f} . \qquad (12)$$

If the charge distribution is uniform, then it is easy to see that test particles incident on the bunch with $b < R$ will be focused to the axis after traveling a distance σ_z/D. As will be discussed in Section III, the behavior of the test particles is actually periodic with a wavelength $\lambda \simeq 4f$ which is related to the bunch plasma frequency. For small values of D, however, viewing the collision in terms of a thin lense with a fixed focal length gives a good physical picture of the test particle dynamics.

A test particle traveling through a non-uniform charge distribution sees a focal length which may change as a function of time due to the variation of the charge density along the collision axis. The effective focal length can also depend on the initial position and angle of the test particle trajectory. If the charge distribution does not differ too

much from a uniform one, this represents a lens with small aberrations, and the point focus of the uniform lens becomes a line focus or a diffuse focus. The disruption factor can still be defined in terms of the focal length for small displacements from the collision axis or equivalently the focal length determined by the central density. For a Gaussian distribution in x, y, and z one has

$$D_x = \frac{2N r_e \sigma_z}{\gamma\sigma_x(\sigma_x + \sigma_y)}$$
$$D_y = \frac{2N r_e \sigma_z}{\gamma\sigma_y(\sigma_x + \sigma_y)} \qquad (13)$$

Note that if the aspect ratio of the beam is not one, the focal lengths in the x and y directions are not equal and one must define two disruption parameters. For the Gaussian case with aspect ratio $\sigma_x/\sigma_y = 1$, the disruption parameter is simply

$$D = \frac{N r_e \sigma_z}{\gamma\sigma_x^2} \qquad (14)$$

The problem becomes much more complex when one considers the collision of two charge distributions. The complication arises because each distribution will be modified during the collision by its interaction with the other one. The disruption factors of the two beams can still be defined in terms of their initial density distributions and the results discussed previously for test particles are obtained when one of the beams is weak and its disruption of the strong beam can be neglected. For the general case however, the focal strength experienced by particles varies with time both because of the variation of charge density along the collision axis and because of the variation in density due to the time dependence of the charge distribution.

The object of colliding intense relativistic beams of positrons and electrons is, of course, to study the fundamental interactions of these particles. When an individual positron and electron annihilate or have a close collision, new particles are produced with a rate that is given by the interaction cross section times the incoming flux. The rate of particle production per unit interaction cross section is called the luminosity and is the quantity which together with the energy determines the usefulness of the machine for the experimenters. The total luminosity is the luminosity per collision multiplied by the number of collisions per second. Hence

$$\mathscr{L} = f\int \rho_1(x,y,z,t)\ \rho_2(x,y,z',t)\ dx\,dy\,dz\,dt \tag{15}$$

where $z' = z - ct$ and f = collision frequency. Neglecting the dynamic changes in the beam density distributions, one can define a luminosity for the limit in which the disruption parameters are zero which is

$$\mathscr{L}_0 = f\int \rho_1(x,y,z,t=0)\ \rho_2(x,y,z',t=0)\ dx\,dy\,dz\,dt \tag{16}$$

For two Gaussian distributions with $\sigma_{x_1} = \sigma_{x_2}$, $\sigma_{y_1} = \sigma_{y_2}$, $\sigma_{z_1} = \sigma_{z_2}$ we get the well known result

$$\mathscr{L}_0 = \frac{N^2 f}{4\pi\ \sigma_x \sigma_y} \tag{17}$$

The factor $1/4\pi\,\sigma_x\sigma_y$ comes only from the x and y integration.

In order to calculate the effects of beam dynamics for arbitrary initial density distributions and investigate any shape dependence, one needs to define the collision strength in a shape independent way. If the charge distribution is characterized by the scale parameters λ_x, λ_y, and λ_z, the variables in the problem can be scaled since we are dealing essentially with a collisionless plasma (point-like scattering). If the variables are now scaled such that

$$\xi_x = x/\lambda_x$$

$$\xi_y = y/\lambda_y \tag{18}$$

$$\xi_z = z/\lambda_z$$

and a shape distribution ρ_ξ is defined using

$$\int \rho_\xi \, d\xi_x \, d\xi_y \, d\xi_z = 1 \ , \tag{19}$$

the luminosity becomes

$$\mathscr{L} = \frac{f N_1 N_2}{\lambda_x \lambda_y} I_0 \tag{20}$$

where I_0 is the overlap integral in x and y and the convolution in z of ρ_ξ with itself. For a Gaussian distribution

$$\rho_\xi = \frac{1}{(2\pi)^{3/2}} e^{-\left(\xi_x^2/2 + \xi_y^2/2 + \xi_z^2/2\right)} \tag{21}$$

and $\lambda_x = \sigma_x$, and $I_0 = 1/4\pi$.

We now must consider the way in which the dynamics scales. For a unit charge, the scattering angle per unit length is given by

$$\frac{dx'}{dz} = \frac{-r_e}{\gamma} \int \rho(x,y,z) \frac{\underset{\sim}{b} \cdot \hat{x}}{b^2} \, dx \, dy \tag{22}$$

where b is the impact parameter of the test charge relative to the element dx dy. This equation can be rewritten in terms of the scale independent variables and the shape distribution as

$$\frac{d^2x}{dz^2} = \frac{-r_e}{\gamma} \frac{N}{\lambda_x \lambda_y \lambda_z} \frac{\lambda_x \lambda_y}{\lambda_b} \int \rho_\xi \frac{\underset{\sim}{\xi_b} \cdot \hat{x}}{\xi_b^2} \, d\xi_x \, d\xi_y \tag{23}$$

and

$$\frac{d^2\xi_x}{d\xi_z^2} = \frac{-r_e}{\gamma} \frac{N \lambda_z}{\lambda_x \lambda_b} \int \rho_\xi \frac{\underset{\sim}{\xi_b} \cdot \hat{x}}{\xi_b^2} \, d\xi_x \, d\xi_y \tag{24}$$

where

$$\underset{\sim}{\xi}_b = \left((x - b_x)/\lambda_x \ , \ (y - b_y)/\lambda_y\right)$$

which is in the form of a dimensionless constant times a shape dependent function. For a Gaussian distribution this has the simple form

$$\frac{d^2\xi_x}{d\xi_z{}^2} = -D\xi_x \, e^{-\xi_x^2/2} \tag{25}$$

for $\xi_x << 1$ and $\xi_y << 1$, or

$$\frac{d^2\xi_x}{d\xi_z{}^2} = -D\xi_x$$

near the bunch center. D is now defined to be

$$D_x \equiv \frac{r_e}{\gamma} \ \frac{N \lambda_z}{\lambda_x \lambda_b} \tag{26}$$

The unperturbed luminosity is related to D by

$$\mathscr{L}_0 = \frac{D_y P}{8\pi mc^2 r_e \sigma_z} \left(\frac{1 + R}{R}\right) \tag{27}$$

where P is the power required to accelerate the beam

$$P = f N \gamma mc^2$$

and R is the aspect ratio

$$R = \frac{\sigma_x}{\sigma_y} \ .$$

Expressing the luminosity as a function of D in this way is only approximate because the effect of the beam dynamics on the overlap integral (i.e., the difference between $\mathscr{L}_0$ and $\mathscr{L}$) has been neglected in calculating the luminosity, but it does point out that if the amount of beam power available is fixed, one must increase the severity of the collision in order to achieve higher luminosities. Note that increasing D by increasing

σ_z without affecting the transverse dimensions has no effect on $\mathscr{L}$ except through beam dynamics.

For the Gaussian shape, the numerical value of the disruption parameter is

$$D = \frac{14.4\, N \sigma_z}{E \sigma_x \sigma_y} \tag{28}$$

where

N = number of particles in units of 10^{10}

σ_z = bunch length in mm

E = beam energy in GeV

$\sigma_x \sigma_y$ = transverse dimensions in microns.

For oppositely charged beams, the first order effect of the beam dynamics is to decrease the transverse dimensions of the beam. Since $\delta r/r$ is proportional to D and the luminosity is proportional to $1/\langle r \rangle^2$ we expect the luminosity to be modified by a factor

$$\frac{\mathscr{L}}{\mathscr{L}_0} \sim \frac{r_0^2}{\langle r \rangle^2} \tag{29}$$

After a distance ℓ, $\delta r/r = - D\ell/\sigma_z$ for $D\ell/\sigma_z < 1$. The dimensions of the opposite beam are also changing so that $D(t) \simeq D_0 (r_0/r)^2$. We have

$$r^2 \simeq r_0^2 \left(1 - \frac{D\ell}{\sigma_z}\right), \qquad \frac{D\ell}{\sigma_z} < 1 \tag{30}$$

and if L is the total length,

$$\begin{aligned} \langle r \rangle &= \frac{1}{L} \int_0^L r_0 \left(1 - \frac{Dz}{\sigma_z}\right)^{1/2} dz \\ &\simeq r_0 \left(1 - \frac{3}{8} \frac{DL}{\sigma_z}\right) . \end{aligned} \tag{31}$$

Hence for $D \sim 1/2$, $L/\sigma_z \sim 2$, and $DL/\sigma_z \sim 1$, the luminosity is enhanced by $\frac{\mathscr{L}}{\mathscr{L}_0} \sim 2.5$.

From eq. (10), the scattering angle distribution for $\sigma_x = \sigma_y$ and impact parameter b is

$$N(\theta) \simeq \frac{N r_e b}{\gamma \sigma_x^2} \frac{N(b)}{N} = \frac{b}{\lambda_z} D \frac{N(b)}{N} \tag{32}$$

which has a maximum near $b \approx \lambda_x$ since for larger impact parameters $N(b)/N$ is decreasing and the scattering angle is less than D/λ_z due to the non-uniformity of the current density. The scattered beam will have a maximum opening angle near λ_x/λ_z D. This opening angle is not a scaling parameter, and its value will depend on the way in which D is increased. If D is increased by increasing λ_z, then θ_{max} will remain roughly constant. If D is increased by increasing the current or decreasing the transverse scale, then θ_{max} will increase proportional to N or $1/\lambda_x$, respectively. Furthermore, if the value of D is larger than one, the particle trajectories are oscillatory and the distribution of scattering angles must be found by simulation.

III. Relation of D to the Plasma Frequency and Instabilities

It is interesting to compare D to the relativistic transverse plasma frequency of the bunch ω_p which is defined as

$$\omega_p^2 = \frac{4\pi \rho r_e c^2}{\gamma} \tag{33}$$

For a three-dimensional Gaussian distribution with charge Ne, ρ varies with position and so does ω_p. Using ρ_{max} and comparing to D defined in terms of the central density (for simplicity $\sigma_x = \sigma_y$).

$$\rho_{max} = \frac{N}{(2\pi)^{3/2} \sigma_x \sigma_y \sigma_z}$$

$$\omega_{Pmax}^2 = \frac{4\pi \rho_{max} r_e c^2}{\gamma} \tag{34}$$

and one finds

$$D = \frac{N r_e \sigma_z}{\gamma \sigma_x^2} = \frac{\omega_p^2 \sigma_z^2}{c^2} \sqrt{\frac{\pi}{2}} \tag{35}$$

The number of plasma oscillations which occur while traveling a distance L is $n = L/\lambda_p$ and using $L \sim \sqrt{2\pi}\,\sigma_z$ and eq. (35) yields

$$D \sim 8n^2 \ . \tag{36}$$

Thus, $\sqrt{D}$ is a measure of the number of plasma oscillations which occur during the collision. This conclusion could also have been reached from the form of the scaled equation of motion, eq. (25).

The results of a full simulation (see Section V) indicate that the effective phase shift for particles near the axis of a Gaussian beam is actually related to D by

$$D = 10.4\ n^2 \ . \tag{37}$$

If the beam behavior was stable for two full plasma oscillations, then D could be as large as 32 for Gaussian beams. Beam growth due to plasma instabilities typically requires several plasma oscillations so that values of D less than 10 are certainly stable. The value of numerical coefficient is somewhat shape dependent.

The collision strength parameter used for storage ring machines is the linear tune shift[3)]

$$\Delta\nu_y = \frac{r_e}{2\pi} \frac{N \beta_y^*}{\gamma \sigma_y (\sigma_x + \sigma_y)} \tag{38}$$

where β^* is the betatron function at the collision point. Using eq. (4) one finds

$$\Delta\nu_y = \frac{D_y}{4\pi} \frac{\beta^*}{\sigma_z} \tag{39}$$

Maximum luminosity is achieved when $\beta^* \sim \sigma_z$ and the observed limitation for the tune shift of $\Delta\nu \sim 0.06$ corresponds roughly to a disruption

parameter of one. This low value is probably a consequence of the fact that there are many collisions in a storage ring per damping time. For this case, Uhm and Liu[4] have derived a dispersion relation for the linearized Vlasov-Maxwell equations which predicts a maximum growth rate of $0.6\ \omega_p$. As pointed out by B. Zotter,[5] this value agrees well with the observed limitation of $\Delta\nu$ using an effective bunch length $L = 2\sqrt{\pi}\ \sigma_z$ but does not explain the fact that the limit is independent of β^*.

The growth of the kink (or hose) instability for the linear collider case has been analyzed by Fawley and Lee[6] who find that the growth factor is limited by the finite length of the interaction to

$$g < \frac{1}{1 + \alpha/2}\,\frac{\omega_\beta\ \ell}{2c} \tag{40}$$

where $\alpha \approx 0.18$ is a term used to model phase mix damping, ℓ is the effective length and ω_β is the effective betatron frequency of the collision. Since $\omega_\beta\ \ell/2c = 2\pi n$, we can use $n \approx \sqrt{D}\,/3.22$ to get (for the Gaussian)

$$g < 1.8\sqrt{D} \tag{41}$$

For a given fractional transverse offset δ, the condition $g\delta < 1$ places a limit on D which is

$$D < \left(\frac{1}{1.8\delta}\right)^2 \tag{42}$$

For a 10% offset this requires that D be less than 31, and for a 25% offset, D must be less than 5.

The effect of the beam emittance on the collision depends on the ratio of the beam envelope size to the Debye length. The Debye length λ_D is the average distance which a particle travels in the transverse dimension during a time $1/\omega_p$.

$$\lambda_D = \frac{\langle v_\perp^2 \rangle^{1/2}}{\omega_p} \tag{43}$$

Hence, if the transverse size of the beam is comparable to λ_D and the collision time is of order $1/\omega_p$, particles will traverse the beam due to emittance effects during the collision, and this will damp any change in the beam envelope due to the coherent focusing effect of the beams. The emittance is the area of the phase space ellipse $\pi\langle x\rangle\langle x'\rangle$ and hence

$$\varepsilon^2 = \pi^2 \lambda_x^2 \frac{\langle p_\perp^2 \rangle}{p^2} = \frac{\pi^2 \lambda_x^2 \langle v_T^2 \rangle}{2c^2} \tag{44}$$

The velocity distribution also defines an effective temperature for the beam which is

$$k T_{eff} = \frac{p_\perp^2}{2\gamma m} = \frac{\varepsilon^2 \gamma m c^2}{2\pi^2 \lambda_x^2} \tag{45}$$

The temperature and the rms velocity actually vary with position within the beam since they depend on the phase space distribution function. Usually the temperature falls to zero on the edges of the beam envelope (where $\langle v_\perp \rangle \approx 0$) and reaches a maximum on the beam axis. For a uniform radial dependence of the temperature

$$\begin{aligned} \langle kT \rangle &\simeq \frac{\varepsilon^2 \gamma mc^2}{4\pi^2 \lambda_x^2} = 1/2\, \gamma m \langle v_\perp^2 \rangle \\ \langle v_\perp^2 \rangle^{1/2} &= \frac{\varepsilon}{\pi} \frac{c}{\sqrt{2}\lambda_x} \end{aligned} \tag{46}$$

The relationship between the beam size and the Debye length for a fixed disruption parameter is found using $D = 1/4\pi\, \omega_p^2 \lambda_z^2/c^2$ and eq. (43)

$$\frac{\lambda_D}{\lambda_x} = \frac{\varepsilon}{\pi} \frac{\lambda_z}{2\sqrt{2\pi}\, \lambda_x^2 \sqrt{D}} \tag{47}$$

When λ_D is much smaller than λ_x the emittance of the beam can be ignored.

IV. Computer Simulation

The computer simulation of the beam-beam effect in a single pass collider is considerably simplified by the fact that the beams are highly relativistic and that the collision occurs only once. For the relativistic beam, the effect of the longitudinal excitation is unimportant, and the transverse motion is given by integrating the effect of the kicks defined by eq. (24). In contrast, the computer investigation of beam-beam effects in a storage ring requires that one follow the evolution of the bunches for a time comparable to the damping time. This time is typically much longer than the time between collisions, and in this case, small perturbations in the initial configuration of the bunches can grow with time and eventually become important. This is difficult to study with a computer because numerical approximations and truncation errors lead to a cumulative loss of information about the beam behavior. The long-time scale also means that longitudinal modes in the beam can be important. The single pass beam-beam effect at high energy can be reliably calculated because of the validity of the impulse approximation and the small number of plasma oscillations for reasonable collision strengths.

The computer simulation used here starts by distributing the charge on a three-dimensional lattice which defines typically 8000 cells for each beam. The central position and trajectory of each cell is advanced using time symmetric difference equations derived from eq. (24). The advantages of time symmetric equations have been discussed by Buneman.[7] In this application, they allow one to verify that the code is reversible and increase the accuracy of the simulation. Any irreversibility is due to round-off errors and coarse binning of the density or time step.

The cells are advanced longitudinally at a uniform velocity equal to the speed of light. For each time step, the transverse kick given to each cell of one beam is calculated from the charge in the cells of the other beam which are at the same longitudinal position. The charge distribution of each beam is modified due to the cumulative effect of all the transverse kicks which have been applied previously.

To further increase the accuracy of the simulation, the charge in each cell is treated as a cloud of charge rather than as a point charge. Simulations in plasma physics often use the particle-in-cell method[8] which simulates the motion of the plasma by having many particles within the cell which share the charge. The number of such particles must be large enough to reduce the particle or shot noise introduced by statistical fluctuations. Real plasmas contain large numbers of particles, and such fluctuations are unphysical. The major advantage of such an approach is that the simulation of temperature effects is simplified since the particles can be given an initial velocity distribution within the cell. The cell is used in these calculations to bin continuous quantities like pressure, density and electromagnetic fields. The density distribution, for example, is calculated by simply counting the number of particles which are found in a given cell at each time step.

The shot noise contributions of the particle-in-cell model can be eliminated by treating each particle as a cloud of charge. As pointed out by Birdsall and Fuss,[9] this cloud-in-cells method also reduces many fictitious effects which come about because of the finite cell size. Errors in time due to the early or late arrival of a particle in a cell and errors in the forces due to the uncertainty of the particle's position

within the cell are smoothed. The finite size cloud also smooths the interactions between particles and eliminates the necessity of cutting off the singularity in the interaction which occurs when point particles approach zero separations.

The cloud size does not have to be equal to the cell size. If it is larger than a cell size or if the cloud is not centered on a cell, the charge is spread out over several cells in proportion to the fraction of the total cloud's area which falls in that cell. If the cloud is smaller than a cell, the model is very similar to the particle-in-cell model with a particular choice for the cutoff distance for the interaction of the charges.

In this simulation, the cloud size is changed as the interaction progresses. The size of a cloud at any given time is determined by the distance to adjacent clouds on a lattice. Using the nearest neighbors to determine the cloud size is equivalent to a first order Taylor series expansion of the motion about the center of the cloud. A fixed cell size is used to calculate the density distribution and the luminosity overlap integral. The cloud's charge is apportioned to the cells using an area weighting scheme.

By dividing each cell into four subcells, the gradient of the density distribution within a cell can be adjusted to match the local gradient measured by the positions of the nearest neighbor clouds. This increases the number of effective cells in the calculations for the purpose of calculating density distributions and overlap integrals of the type given by eq. (15) without increasing the number of clouds which must be followed in the simulation of the dynamics. At the expense of increased computing

time, several clouds can be superimposed at the same positions but with differing velocities to simulate temperature effects, but we concentrate here on the cold beam limit. The cell size is usually equal to the original cloud size since the behavior of the beam is not followed on a scale smaller than a subcell. A cell size larger than the original cloud size would decrease the accuracy of the luminosity calculation.

V. Results of the Simulations

Consider the collision of two beams with Gaussian profiles and scale factors σ_x, σ_y, and σ_z. One can begin studying the effect of the collision by looking at the motion of a test charge in one beam whose position (x,y,z) relative to the center of the beam is (σ_x, 0, 0). The trajectories in the x,z projection for increasing values of the collision strength are shown in fig. 5. As can be seen in fig. 5 for the case D = 1, the effect of beam 2 on this test charge is well represented by a focal length which is equal to the bunch length σ_z. For large values of D, it is best to think in terms of the number of betatron oscillations which a particle executes as it passes through the other beam.

The case D = 1 corresponds roughly to a quarter betatron oscillation and D = 10 is slightly more than one full oscillation. Because of the form of eq. (24), the equation of motion for small offsets from the beam center is given by

$$\Delta\xi_x' \simeq -D\xi_x \tag{48}$$

so that the betatron wave length will be proportional to the square root of D. The observed values for the phase shift of the test particle at $x = \sigma_x$ are shown in fig. 6 and the phase shift is found to be $\Delta\phi \simeq 0.62\pi\sqrt{D}$.

This relationship for the focal strength of the beam works well up to quite large values of the collision strength and agrees reasonably with the rough calculation of Section III, eq. (36). The corrections due to the changes which occur in the other beam are small. The exit angle versus position of the test charge for D between 0 and 32 is shown in fig. 7. The position is that which occurs when the longitudinal separation between the two beams is 2.5 σ_z. This corresponds to a position for beam 1 of z/σ_z = 1.25 in fig. 5. As D increases from 0 to 1, the exit angle increases. The maximum exit angle occurs when D is between 1 and 2. The values of test charge exit angle and position for increasing values of D form an approximate ellipse similar to a phase ellipse. The rotation of the ellipse is related to the effective thickness of the lens. The positions of the points for D = 16 and D = 32 are close to those for D = 3 and D = 8 respectively and indicate that the nonlinearities of the interaction are not very important.

Due to the fact that the charge distributions of the beams change during the collision, the dynamics of the leading and trailing parts of the beam are not quite the same as those of the central part. Figure 8 shows a superposition of the trajectories in the xz plane of all the lattice points with y = 0 for the case where D = 2.4. The lattice is 10 × 20 in this projection and the distance between lattice points is 0.5 σ_z. The trajectories should be compared to fig. 5 for the case D = 2. Particles within 1 σ of the beam center are scattered through the maximum angle. The particles scattered through small angles come predominantly from the trailing part of the beam which scatters off a partially disrupted charge distribution and therefore sees a smaller charge density.

Figures 9a-c show the density in the y = 0 plane of one of the beams for the case D = 1, 3, and 5. The times shown are in arbitrary units corresponding to a beam center-to-center separation of 10 σ_z at T = 0 and T = 40. The longitudinal positions of the beam centers coincide when T = 20 and the luminosity overlap integral (eq. (15)) receives most of its contributions from 15 < T < 25.

By comparing fig. 9a, 9b, and 9c, one can see that as D is increased from 1 to 5, the focal point of the beam moves toward smaller times. For D = 1, 3 and 5, the focus occurs near T = 26, T = 18, and T = 16 respectively. In all cases the focus is diffuse because of the non-uniform charge distribution. As expected, the transverse tails have longer focal lengths.

The luminosity will reach a maximum when the focal spots of the two beams overlap most completely, i.e., when the central focus occurs near T = 20. This happens near D = 2.4. The harmonic motion of particles near the center for D > 2 (see fig. 5) can yield several diffuse foci during beam collisions (see fig. 9c, T = 25).

As discussed in Section II, the luminosity overlap integral will be a function of D because of the time dependence of the density distribution caused by the beam disruption. For oppositely charged beams which are not too severely disrupted, the dynamics lead to an enhancement of the luminosity. Using the time dependent density distributions found by the simulation, this enchancement can be studied as a function of the collision strength. The enhancement is defined as the ratio between the actual luminosity (eq. (15)) and the unperturbed luminosity (eq. (16)) and is

shown in fig. 10. In order to accurately calculate the overlap integral, the number of lattice points used in the simulation must be large enough to follow the density variations during the collision. The integral is calculated directly from the density distribution of the two beams at each step. The dependence of the enhancement factor on the cell size was investigated and the number of cells was increased until no further effect of the cell size could be seen.

VI. Offset Beams and Uniform Transverse Profiles

For the case where the density distributions do not change (the limit as D goes to zero), one can calculate the effect of an initial offset of $n\sigma$ in the transverse plane on the luminosity. The overlap integral (eq. (16)) gives a luminosity

$$\mathscr{L} = \frac{e^{-n^2/4}}{4\pi} = \mathscr{L}_0 e^{-n^2/4} \tag{49}$$

for Gaussian beams. The luminosity as a function of D for n = 2 is shown in fig. 11. From eq. (49) one can see that for a two sigma offset the D = 0 luminosity is reduced by a factor of 0.37. However, the enhancement still occurs and the ratio of maximum luminosity to D = 0 luminosity is almost the same as in the zero offset case. The enhancement drops off more rapidly with D however.

Similar results have been obtained for the case where the beam has a uniform density profile in the transverse direction and a Gaussian profile in the longitudinal direction. The collision strength is from eq. (26)

$$D = \frac{r_e N \sigma_z}{\gamma \lambda^2} \tag{50}$$

and the unperturbed luminosity is $\mathscr{L}_0 = 1$. The trajectories for test particles are shown in fig. 12 and the enhancement is shown in fig. 13.

For the uniform profile, the enhancement falls off rapidly as the collision strength is increased leading to a net loss of luminosity for D greater than 16. The local peaks in the enhancement correspond to values of the collision strength yielding trajectories which tend to focus the two beams when the maximum charges overlap. (This is the point Z = 0 in fig. 12.)

The more rapid fall-off of luminosity with collision strength for the uniform case can be understood in terms of the plasma properties of the charge distributions. In the leading and trailing parts of a Gaussian beam and in the transverse tails, the charge density is less than the density in the central part of the beam. Since the plasma frequency squared is proportional to the density, this means that the corresponding plasma wavelength λ_p is longer in the tails and that the tails are more stable than the beam core. When beam dynamics are neglected, the tails of the beam contribute little to the luminosity of the collision. The luminosity is proportional to the integral of the density squared and in the Gaussian case, for example, it receives very little contribution from those parts of the beam which are more than one sigma from the center or times when the beams are separated longitudinally by more than one sigma.

When beam dynamics are included, one expects that the cumulative focusing effect of the head of the beam on the central core will be important in determining the approximate transverse dimensions of the beam core and its profile when it overlaps with the core of the other beam. Thus, the charge distribution in the head of the beam is an important factor in determining the enhancement factor or ratio of the actual luminosity to the luminosity expected for undisturbed beam profiles. The

Gaussian transverse profile has a larger enhancement for D > 10 than the uniform profile because the non-uniform density distribution leads to a spread in the plasma frequencies and this together with the longer plasma wavelength in the tails helps stabilize the enhancement factor.

VII. Conclusions

The energy lost per turn by a particle stored in a magnetic ring grows as the fourth power of the particle's energy and this power loss has become a significant constraint in the design of machines to produce high energy electron-positron collisions. This problem has led to the consideration of the properties of alternative systems which collide linearly accelerated beams of electrons with similar beams of positrons. The required luminosity is achieved in a linear system by having very tight focusing at the beam collision point. Spot sizes of several square microns can be achieved.

The beam-beam effect which limits the current which can be stored in a circular machine is still expected to be the limiting factor in linear systems. However, the limitation comes not from the cumulative effect of many small perturbations but from the disruptive nature of a single collision. Particle densities several orders of magnitude higher can be achieved in the single collision case. In addition, the strong disruption of the beams leads to an enhancement of the luminosity due to the net focusing effect which the two oppositely charged beams have on each other (see fig. 1).

The strength of the interaction between the beams $\sqrt{D}$, is related to the number of plasma oscillations which occur during the collision. The plasma frequency however grows only as the square root of the incoming current, and this means that very high beam densities can be tolerated.

Typical instability growth rates would allow several plasma oscillations. For Gaussian beam profiles, two full plasma oscillations occur for $D \approx 32$.

The interaction of two such beams for small numbers of plasma oscillations can be reliably calculated using plasma simulation techniques. The magnitude of the luminosity enhancement and the relation between beam density and effective plasma wavelength have been investigated using a computer simulation. The luminosity enhancement grows proportional to D^2 and reaches a maximum value when the focal spots of the two beams overlap most completely. This occurs after one-quarter plasma oscillation. For Gaussian bunches, the enhancement reaches a maximum for $D \simeq 2.4$ and remains constant to large values of D ($D \approx 20$). The value of the enhancement is approximately 6 for a Gaussian beam which is mismatched at insertion, and 2.5 for a matched beam (i.e., emittance dominated minimum waist). The non-uniformity of the Gaussian charge density helps stabilize the beam dynamics. For more uniform shapes, the enhancement drops off more rapidly with D.

Suggestions for linear colliding beam machines have been limited to small values of the disruption parameter.[10,11] In future designs it should be possible to greatly increase the design luminosity by increasing the collision strength and taking advantage of the luminosity enhancement. A disruption limit $D = 32$ with a luminosity enhancement $\mathscr{L}/\mathscr{L}_0 = 6$ yields an increase in luminosity of

$$D^2 \frac{\mathscr{L}}{\mathscr{L}_0} = 6 \times 10^3$$

if the current is increased or

$$D^2 \frac{\mathscr{L}}{\mathscr{L}_0} = 2 \times 10^2$$

if the beam spot is decreased compared to a design with $D = 1$ and $\mathscr{L}/\mathscr{L}_0 = 1$.

Acknowledgements

The author would like to thank T. Solazzo for assistance with the analysis of the simulation results and B. Richter, E. Lee, and W. Fawley for useful discussions.

This work was supported by the Department of Energy under contract DE-AC03-76SF00515.

References

1. M. Tigner, Nuov. Cim., Vol. 37, No. 3 (1965), 1228; U. Amaldi, Phys. Lett. B61, 313; J.-E. Augustin et al., Proceedings of the Workshop on Possibilities and Limitations of Accelerators and Detectors (Batavia, 1978) 87.
2. J. D. Jackson, Classical Electrodynamics (John Wiley & Sons, Inc., New York, 1962).
3. A. Chao, PEP NOTE 279; B. W. Montague, "Calculation of Luminosity and Beam-Beam Detuning in Coasting Beam Interaction Regions," CERN/ISR-GS/75-36 (1975).
4. H. S. Uhm, C. S. Liu, Phys. Rev. Lett. 43 (1979) 914.
5. B. Zotter, LEP-Note 194, CERN (1979).
6. William M. Fawley, Edward P. Lee, Lawrence Livermore Report, UCID-18584.
7. O. Buneman, Journal of Computational Physics, 1 (1967) 517.
8. R. W. Morse, Methods in Computational Physics 9 (1970) 312.
9. C. Birdsall, D. Fuss, Journal of Computational Physics 3 (1969) 494.
10. J.-E. Augustin et al., Proceedings of the Workshop on Possibilities and Limitations of Accelerators and Detectors (Batavia, 1978) 87.
11. SLAC LINEAR COLLIDER DESIGN REPORT, SLAC Report 229.

Figure Captions

1. Computer simulated collision of intense relativistic beams illustrating the pinch effect.
2. In the rest frame of particle 1, particle 2 travels along the z axis and has a minimum displacement from particle 1 of b in the x direction.
3. Time dependence of the electric and magnetic fields due to the passage of particle 2 as seen at the position of particle 1.
4. Test particle incident with displacement b from the axis of a charge distribution.
5. Trajectory of a test charge incident on a Gaussian bunch with displacement σ_x from the axis for the case D = .5, 1, 2, 5, 10, 32. The test charge is within a Gaussian charge distribution.
6. Phase shift of the test particle versus disruption parameter.
7. Exit angle versus position of the test charge incident at $(\sigma_x,0,0)$ for values of D between 0 and 32.
8. Trajectories of the lattice points in the yz plane for the case D = 2.4.
9. (a),(b),(c) Simulation of the density distributions during the collision of two Gaussian beams for D = 1, 3, and 5.
10. Luminosity enhancement versus disruption factor.
11. Luminosity versus disruption factor for two Gaussian beams colliding with an initial offset of $2\sigma_x$.
12. Trajectory of a test charge incident on a uniform transverse profile, Gaussian longitudinal profile beam. The test charge is initially at the boundary of the transverse distributions and is within a uniform transverse profile beam.

13. Luminosity enhancement versus disruption factor for uniform transverse profile beam collisions.

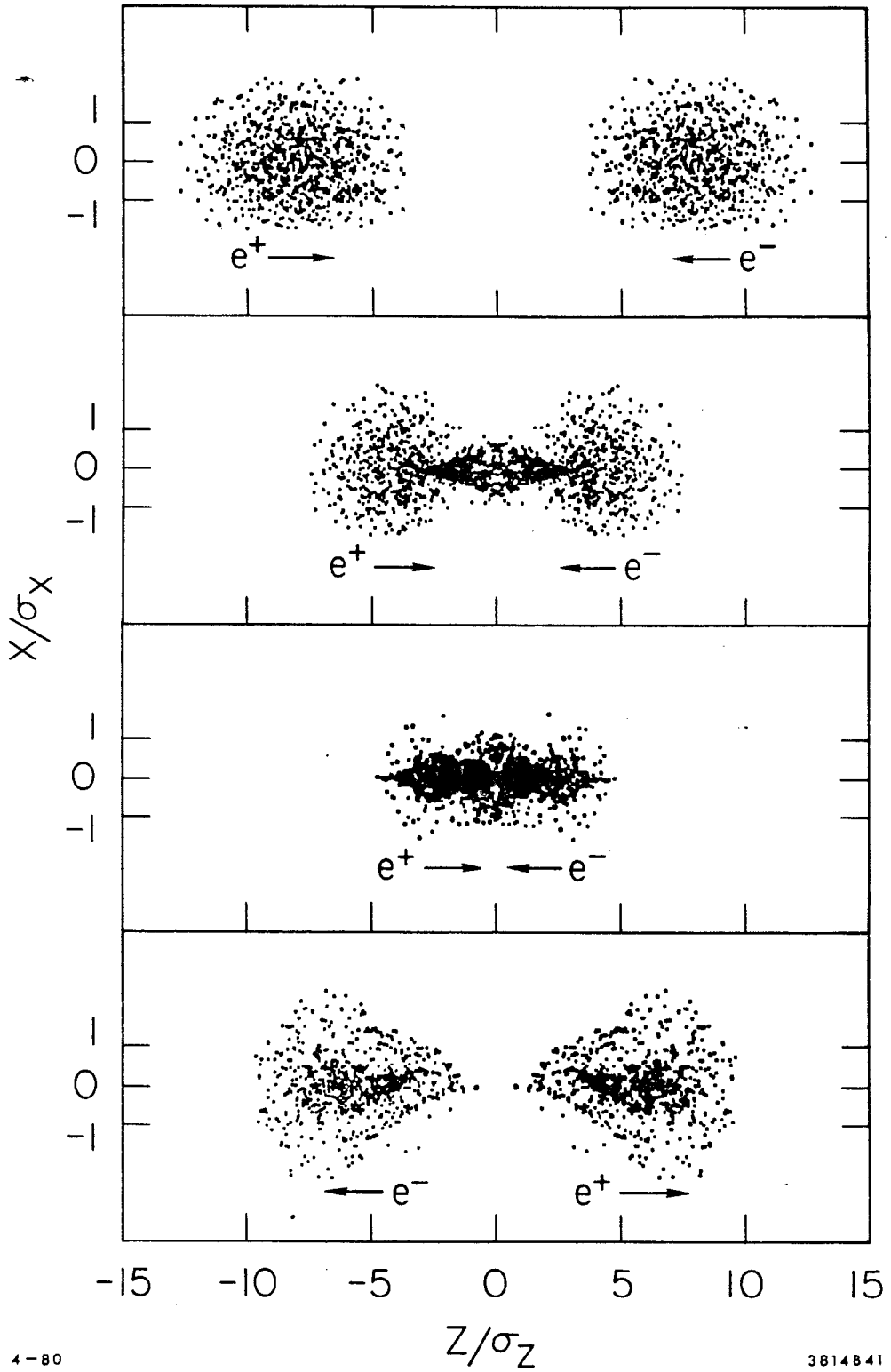

Fig. 1

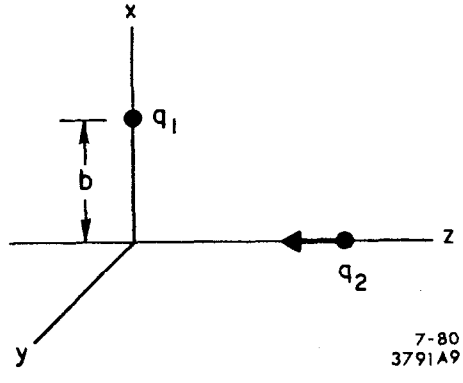

Fig. 2

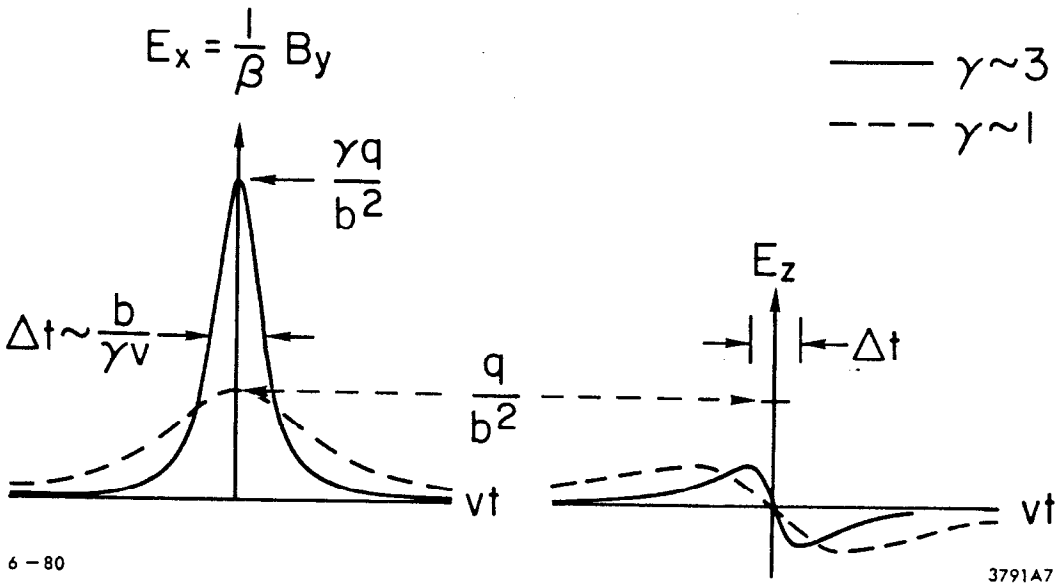
$E_x = \frac{1}{\beta} B_y$
$\gamma \sim 3$
$\gamma \sim 1$
$\frac{\gamma q}{b^2}$
$\Delta t \sim \frac{b}{\gamma v}$
$\frac{q}{b^2}$
vt
E_z
Δt
vt
6 – 80
3791A7

Fig. 3

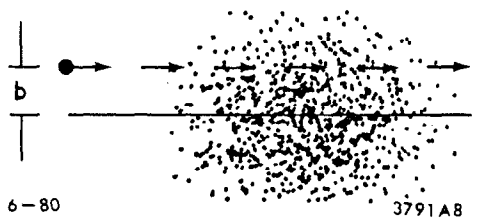

Fig. 4

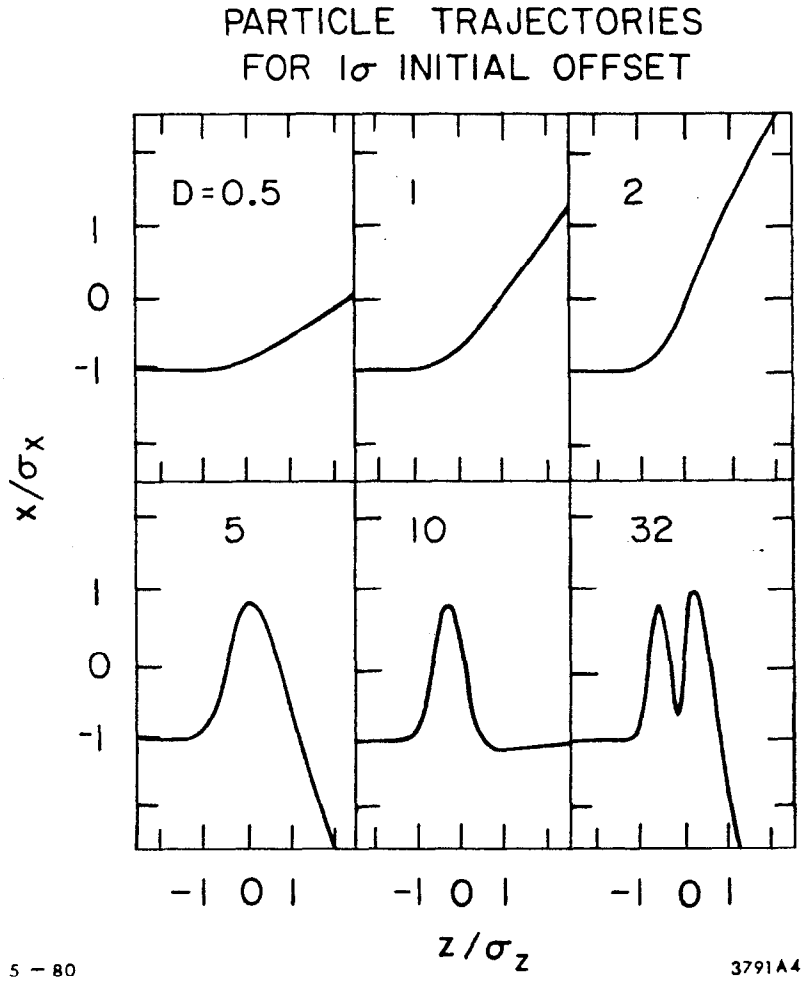
PARTICLE TRAJECTORIES
FOR 1σ INITIAL OFFSET
D=0.5
1
2
5
10
32
x/σx
z/σz
5 – 80
3791A4

Fig. 5

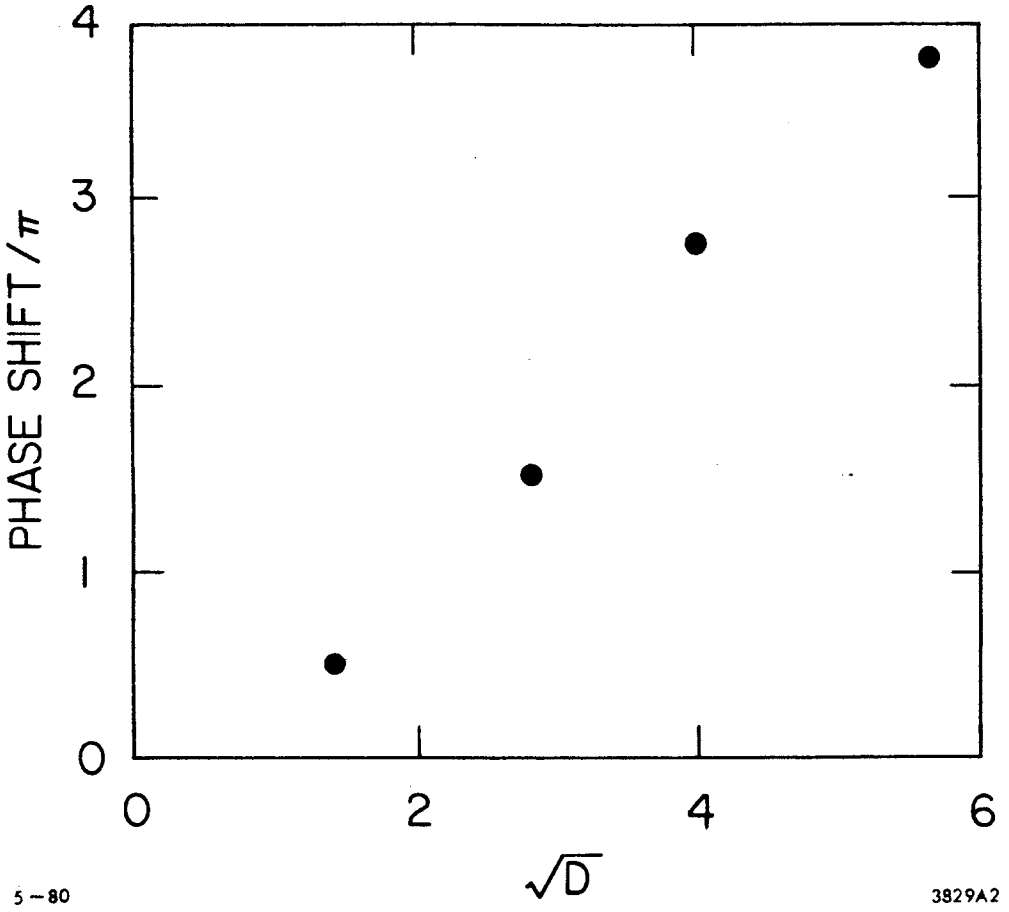

Fig. 6

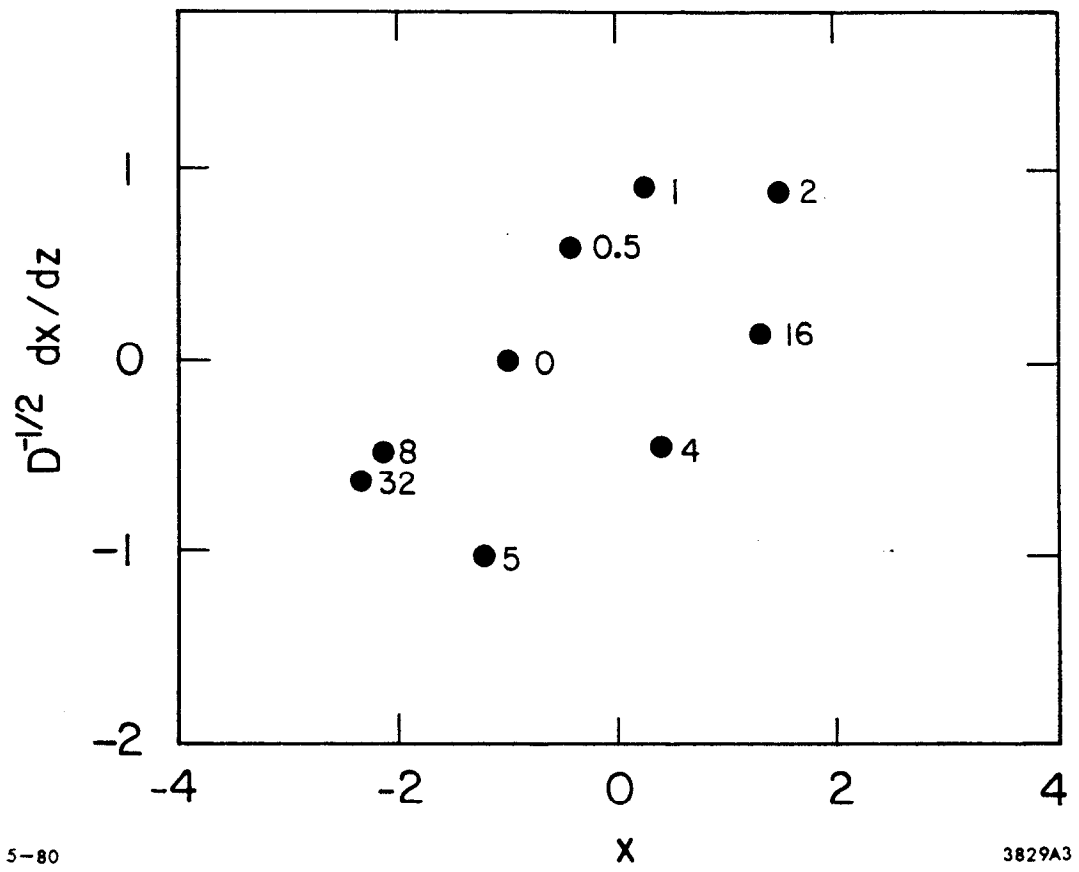

Fig. 7

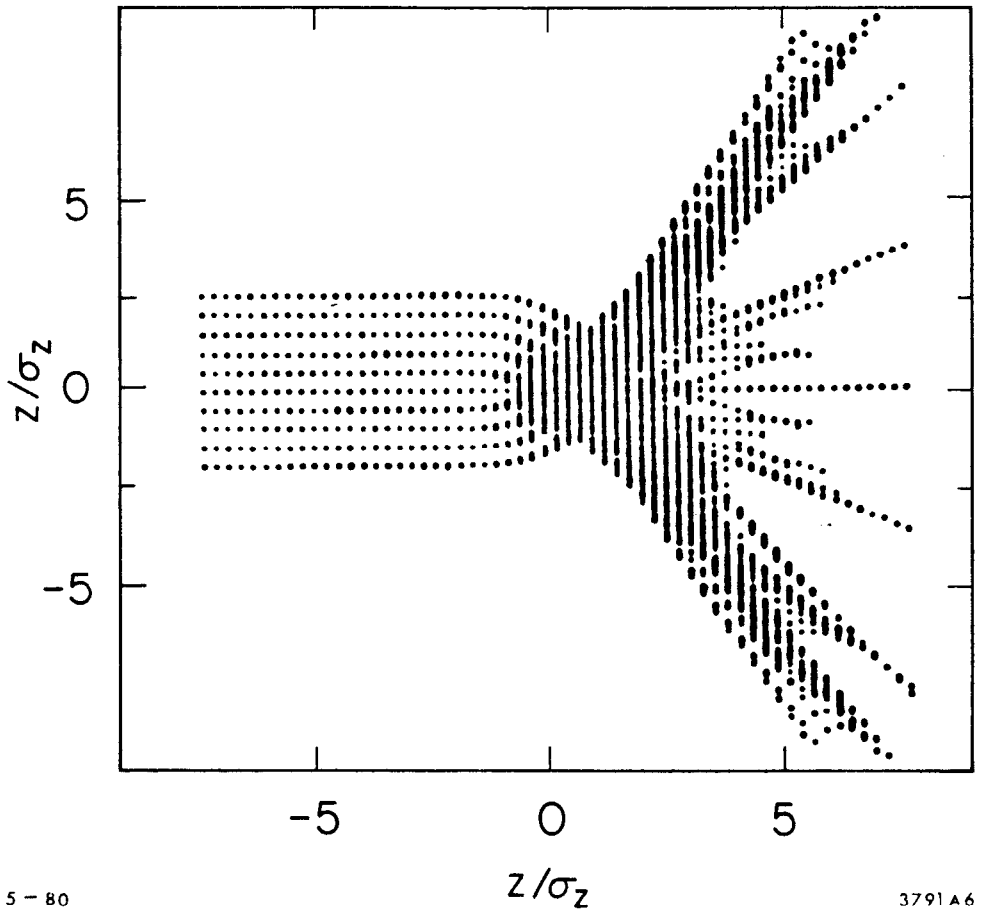

Fig. 8

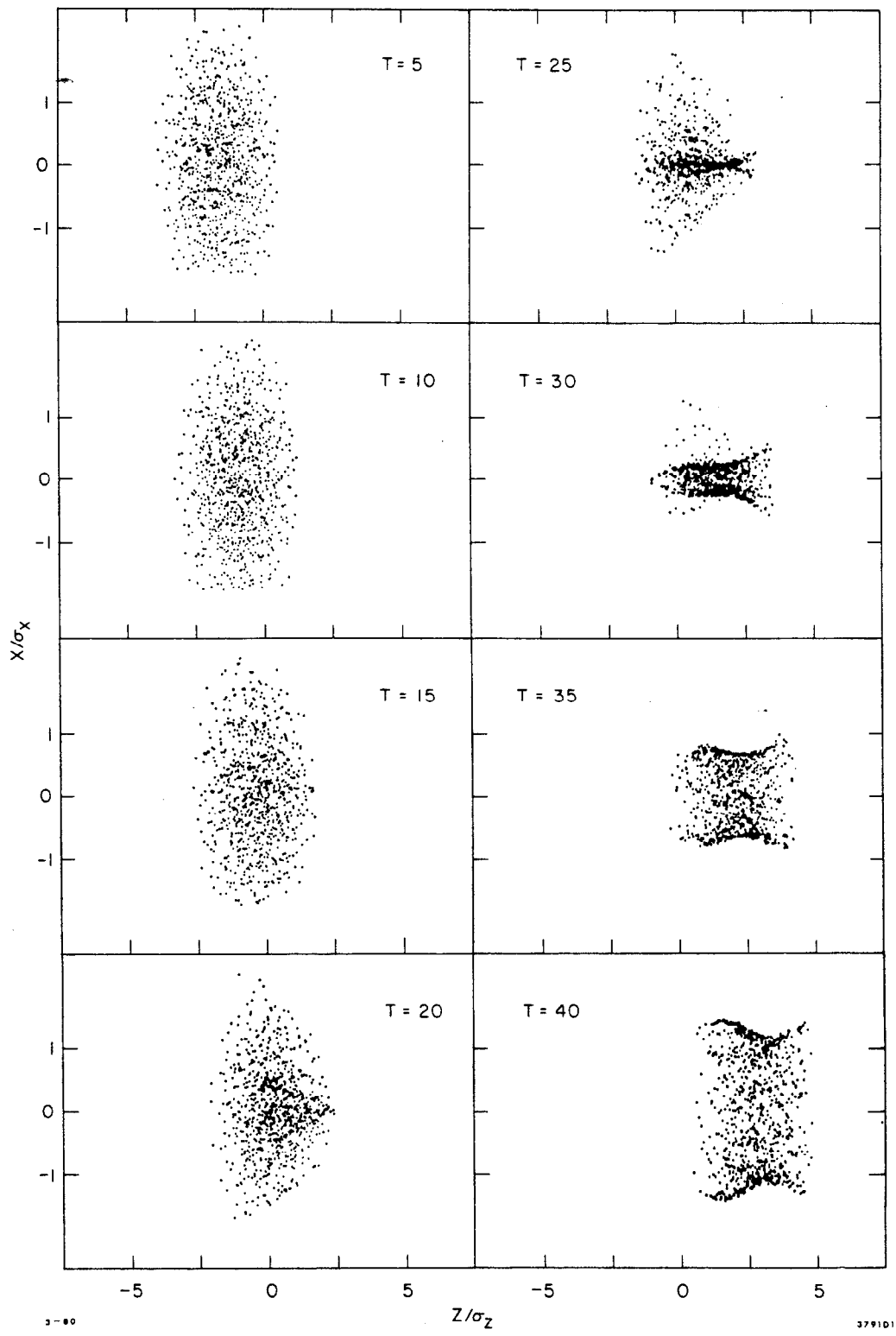

Fig. 9(a)

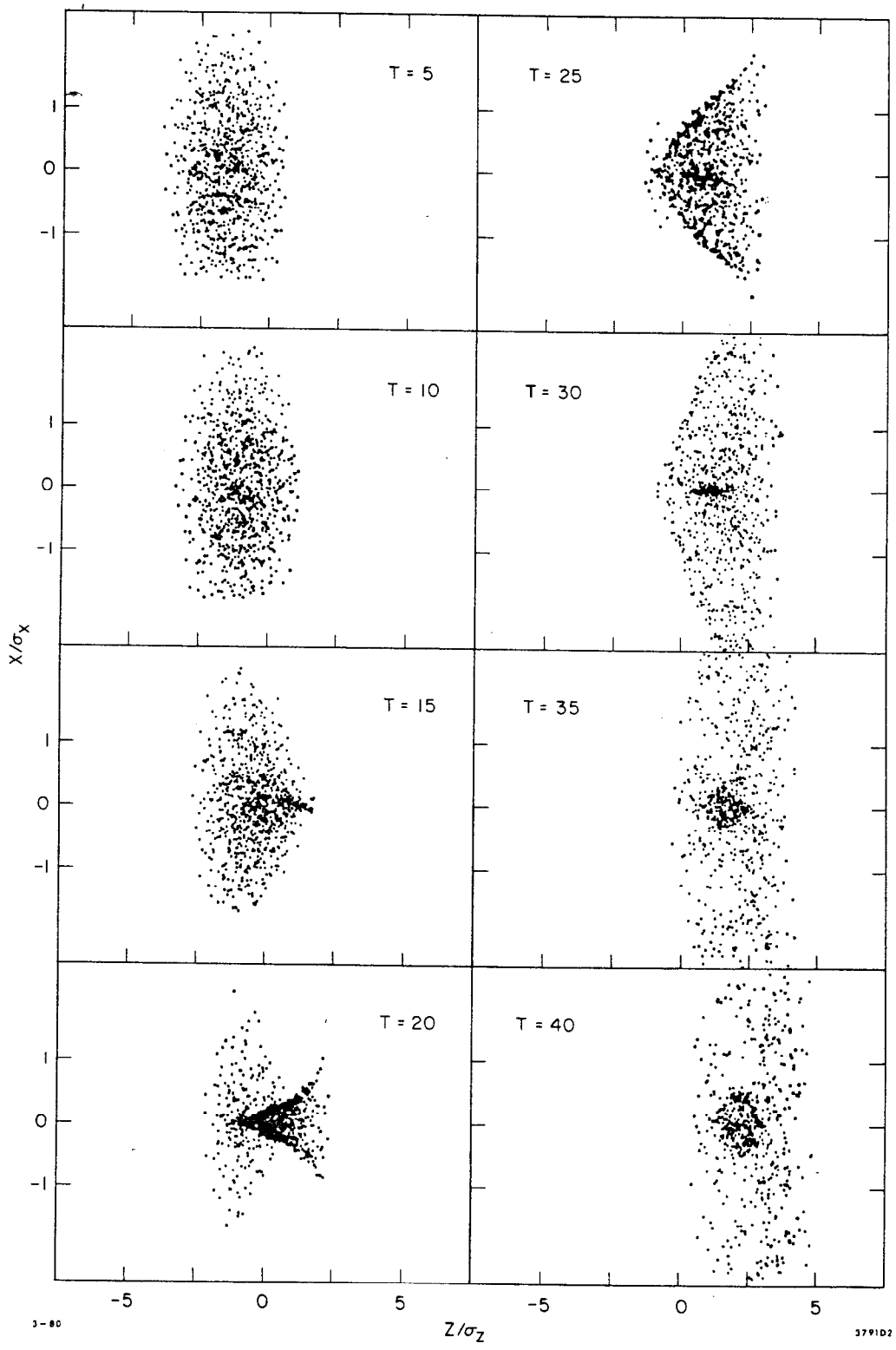

Fig. 9(b)

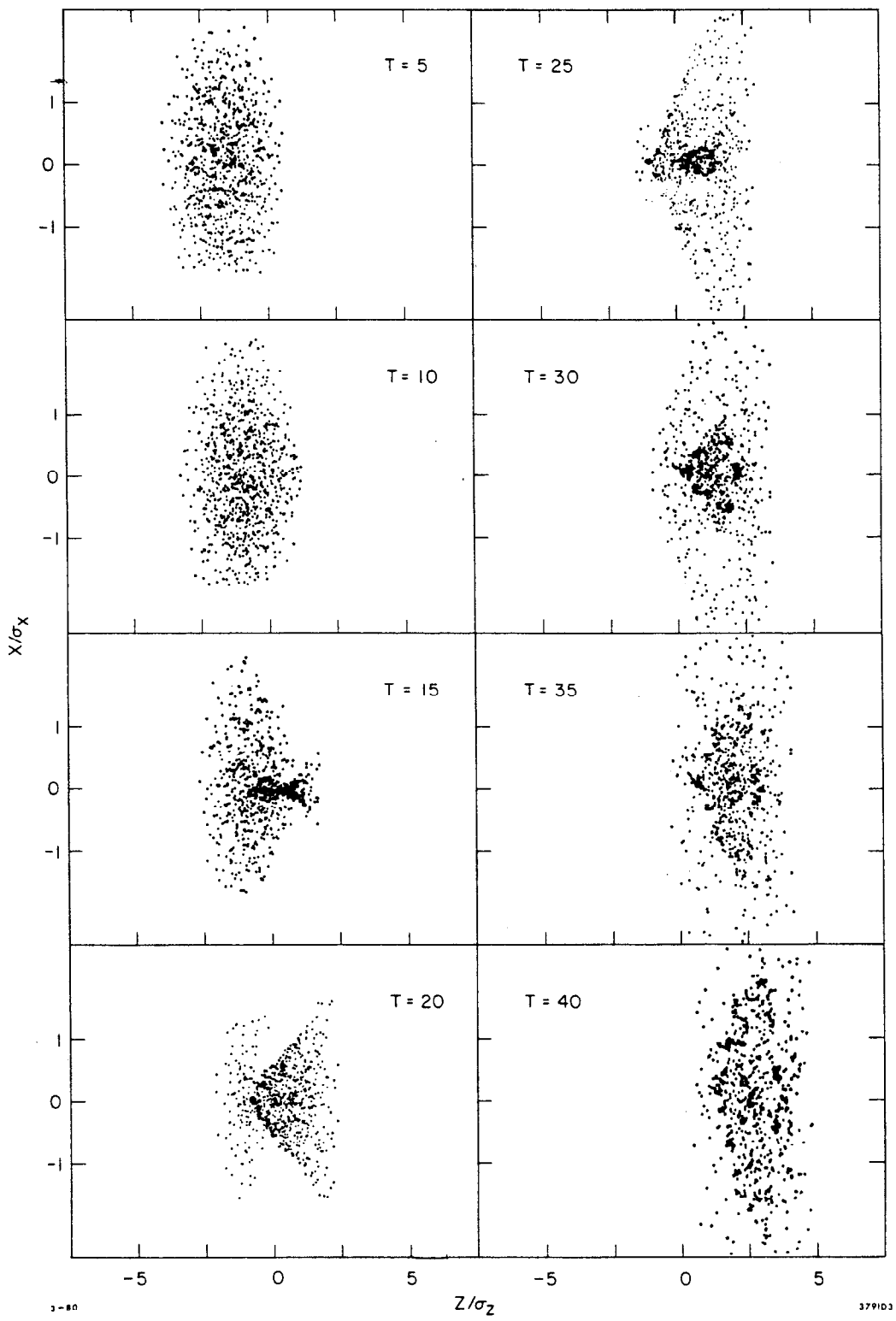

Fig. 9(c)

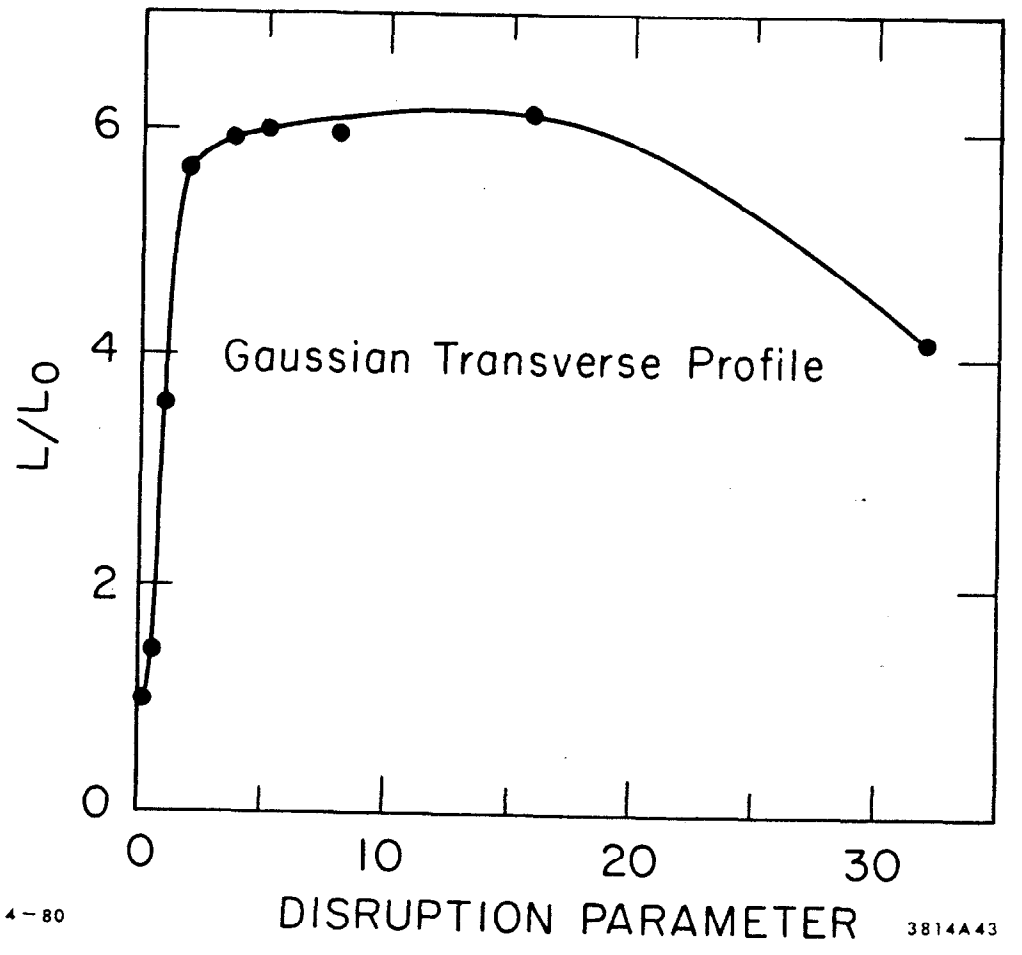
6
4
2
0
L/L0
Gaussian Transverse Profile
0
10
20
30
DISRUPTION PARAMETER
4-80
3814A43

Fig. 10

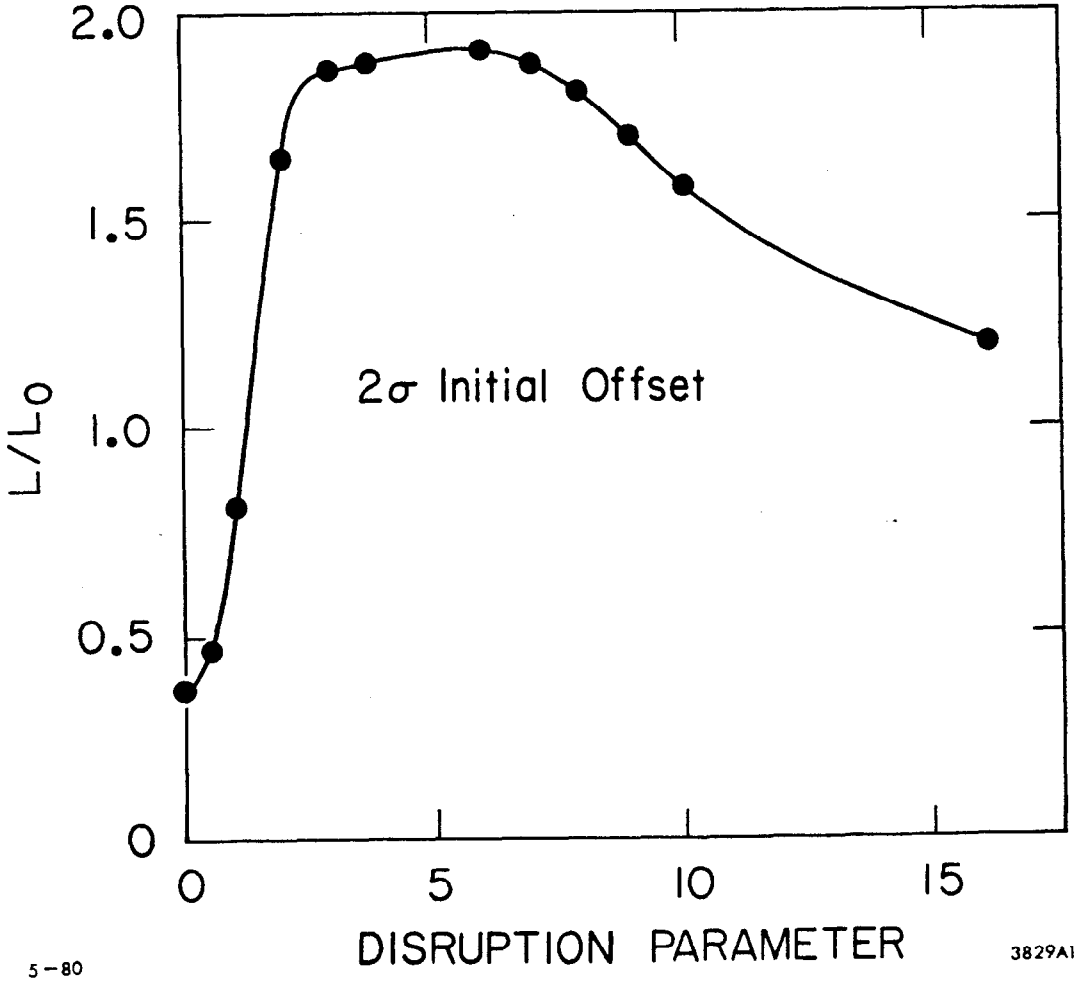
2.0
1.5
1.0
0.5
0
L/L0
2σ Initial Offset
0
5
10
15
DISRUPTION PARAMETER
5-80
3829A1

Fig. 11

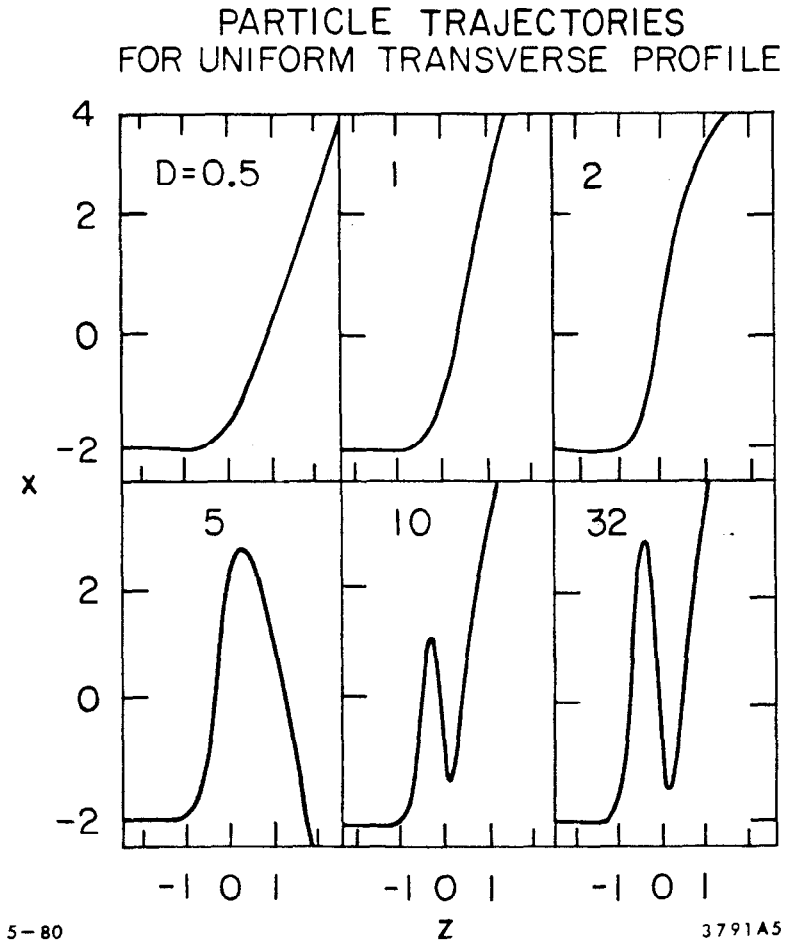
PARTICLE TRAJECTORIES
FOR UNIFORM TRANSVERSE PROFILE
D=0.5
1
2
5
10
32
4
2
0
-2
X
-1 0 1
Z
5-80
3791A5

Fig. 12

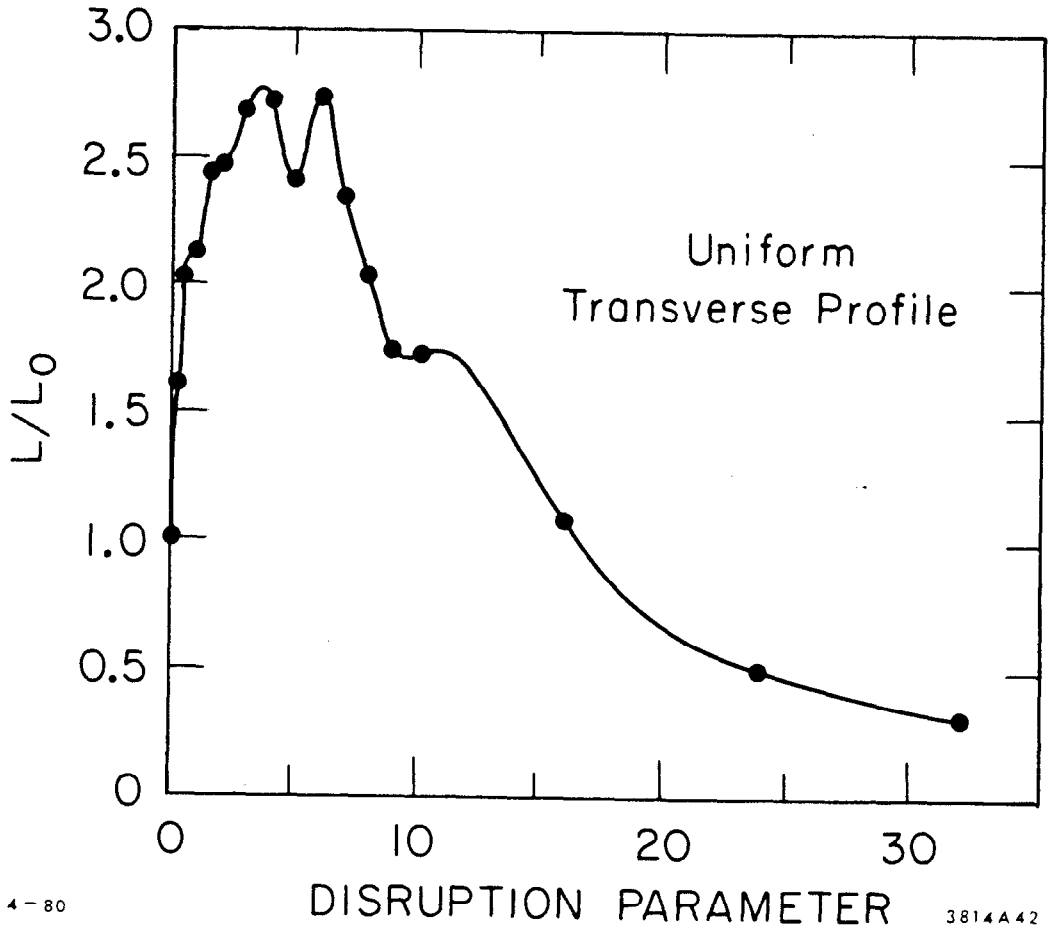
3.0
2.5
2.0
1.5
1.0
0.5
0
L/L0
Uniform
Transverse Profile
0
10
20
30
DISRUPTION PARAMETER
4-80
3814A42

Fig. 13